Published in final edited form as:
J Cell Sci. 2016 April 1; 129(7): 1305–1311. doi:10.1242/jcs.180885.

HDAC6 regulates the dynamics of lytic granules in cytotoxic T lymphocytes

Norman Núñez-Andrade[1,2], **Salvador Iborra**[3], **Antonio Trullo**[4,5], **Olga Moreno-Gonzalo**[1,2], **Enrique Calvo**[6], **Elena Catalán**[7], **Gaël Menasche**[8], **David Sancho**[3], **Jesús Vázquez**[6], **Tso-Pang Yao**[9], **Noa Beatriz Martín-Cófreces**[#1,2], and **Francisco Sánchez-Madrid**[#1,2]

[1]Servicio de Inmunología, Hospital Universitario de la Princesa, UAM, IIS-IP. Madrid, 28006 Spain

[2]Laboratory of Intercellular communication, Fundación CNIC, Madrid, 28029 Spain

[3]Immunobiology of inflammation, Fundación CNIC, Madrid, 28029 Spain

[4]Microscopy and Dynamic Imaging Unit, Fundación CNIC, Madrid, 28029 Spain

[5]Spettroscopia biomedica in fluorescenza dinamica, Center of Experimental Imaging, Ospedale San Raffaele, Milan, 20132, Italy

[6]Proteomic Unit. Fundación CNIC, Madrid, 28029 Spain

[7]Dept. Biochemistry and Molecular and Cell Biology, Universidad de Zaragoza, 500009, Spain

[8]Laboratory of Normal and Pathological Homeostasis of the Immune System, INSERM Unité Mixte de Recherche 1163, Paris France

[9]Departments of Pharmacology and Cancer Biology Duke University, Medical Center, Durham, North Carolina 27710, U.S.

[#] These authors contributed equally to this work.

Abstract

HDAC6 is a tubulin deacetylase involved in many cellular functions related to cytoskeleton dynamics including cell migration and autophagy. In addition, HDAC6 affects antigen-dependent $CD4^+$ T cell activation. In this study, we show that HDAC6 contributes to the cytotoxic function of $CD8^+$ T cells. Immunization studies revealed defective cytotoxic activity *in vivo* in the absence of HDAC6. Adoptive transfer of wild-type or *Hdac6*$^{-/-}$ $CD8^+$ T cells to *Rag1*$^{-/-}$ mice demonstrated specific impairment in $CD8^+$ T cell responses against vaccinia infection. Mechanistically, HDAC6-deficient cytotoxic T lymphocytes (CTLs) showed defective *in vitro* cytolytic activity related to altered dynamics of lytic granules, inhibited kinesin 1 – dynactin mediated terminal transport of lytic granules to the immune synapse and deficient exocytosis, but not to target cell recognition, T cell receptor (TCR) activation or interferon (IFNγ) production. Our results establish

Contact information: Francisco Sánchez-Madrid, Laboratorio de Comunicación Intercelular, Servicio de Inmunología, Hospital de La Princesa, Diego de León 62. 28006, Madrid. Spain, fsmadrid@salud.madrid.org, Phone: +34915202307, FAX: +34915202374.

Author contribution. NNA, NBMC and FSM designed experiments, made the figures and wrote the manuscript; NNA, SI, NBMC, OMG, JV, DS, GM and TSY and EC collected and/or analyzed data; AT developed the Quant Application.

Conflict of interest. Authors declare that they have no conflict of interest.

Europe PMC Funders Author Manuscripts

HDAC6 as an effector of the immune cytotoxic response that acts by affecting the dynamics, transport and secretion of lytic granules by CTLs.

Introduction

Cytotoxic T Lymphocytes (CTLs) are a specialized population of $CD8^+$ T cells that provides defense against virus-infected cells and tumors. Naïve $CD8^+$ T cells differentiate into CTLs upon antigen recognition, a process involving the synthesis and storage of cytotoxic mediators into lysosomal-derived lytic granules (LG) (Williams and Bevan, 2007). CTLs eliminate target cells by different mechanisms, including secretion of pro-inflammatory cytokines, e.g. tumor necrosis factor (TNF)α or interferon (IFN)γ (de Saint Basile et al., 2010), FAS-L (FAS ligand) ligation to its receptor as well as granule-mediated apoptosis upon cell-cell contact and immune synapse (IS) formation (Ritter et al., 2013). LG fuse with the plasma membrane and release granzymes, cathepsins and perforins (Prf) (Lopez et al., 2013; Pardo et al., 2009). The IS acts as a focal point for exocytosis of LG. LG polarization towards the target cell depends on T cell receptor (TCR) engagement, driven by the relocation of the centrosome to IS. The LG degranulate at a secretory domain adjacent to the TCR-enriched region within the IS (de Saint Basile et al., 2010; Ritter et al., 2013).

Histone deacetylase 6 (HDAC6) is an ubiquitous, cytosolic protein from the class II HDACs family with X-linked inheritance, that binds to and deacetylates α-tubulin at lys40 (Hubbert et al., 2002; Valenzuela-Fernandez et al., 2008). HDAC6 also modulates other substrates, e.g. cortactin or hsp90. HDAC6 controls cell migration (Zhang et al., 2007), T-regulatory functions (de Zoeten et al., 2011) and $CD4^+$ T cell activation (Serrador et al., 2004). Consistent with this, HDACs inhibitors impair some immune functions (Mosley et al., 2006; Tsuji et al., 2015). However, the precise contribution *in vivo* (by using *Hdac6*$^{-/-}$ mice) has not been assessed, and the mechanisms involved remain unsolved. HDAC6 also functions as a scaffold protein in T cell migration (Cabrero et al., 2006) and the transport of misfolded proteins (Kawaguchi et al., 2003). In this report, we describe the impaired killing capacity of *Hdac6*$^{-/-}$ CTLs. The molecular mechanism underlying this defect involves a scaffold role that positions HDAC6 as a protein that oversees the proper movement of LG, their transport to the IS and secretion towards the target cell.

Results and Discussion

HDAC6 deficiency reduces the cytolytic capacity of $CD8^+$ T lymphocytes

We examined the ability of cytotoxic T cells from *Hdac6*$^{-/-}$ mice to kill target cells *in vitro*. $CD8^+$ T cells from wild-type (WT) and *Hdac6*$^{-/-}$ mice expressing the transgenic ovalbumin (OVA)-specific TCR (OT-I) were activated *in vitro* and cultured to generate CTLs. Cell cytotoxicity was subsequently analyzed by survival of dye-labeled EL4 target cells pulsed or not with $OVA_{257\text{-}264}$ peptide (SIINFEKL). *Hdac6*$^{-/-}$ CTLs showed decreased killing activity (Fig. 1A), consistent with reduced expression of CD107a (also known as Lamp1) in *Hdac6*$^{-/-}$ CTLs upon degranulation (Fig. 1B). Likewise, CTLs from OT-I mice treated treated with tubastatin A, a potent HDAC6 inhibitor, displayed a reduced killing ability (Suppl. Fig. 1A). We also detected decreased Prf1 secretion from activated (i.e. induced by anti-CD3 and anti-

CD28 monoclonal antibodies) *Hdac6*$^{-/-}$ CTLs (Fig. 1C, left). Next, we assessed the secretion promoted by phorbol-12-myristate-13-acetate (PMA), to bypass TCR stimulation. Both cathepsins D and Prf1 decreased in supernatants from activated *Hdac6*$^{-/-}$ CTLs (Fig. 1C, right). Taken together, our data demonstrate that *Hdac6*$^{-/-}$ CTLs show reduced cytotoxic activity, and suggest that HDAC6 controls exocytosis.

We next tested IFN-γ production; the frequency of CTLs producing IFNγ and its secretion was unaffected in activated *Hdac6*$^{-/-}$ CTLs (Fig. 1D-E), in contrast to what has been described when cells are treated with ACY-1215, a recently described inhibitor that is ten-fold more selective for HDAC6 than for HDAC1, HDAC2 and HDAC3 and that shows slight activity against HDAC8 (Tsuji et al., 2015). Likewise, treatment of CTLs from OT-I mice with tubastatin A had no significant effect (Suppl. Fig. 1B). Importantly, T-cell signaling induced by anti-CD3/anti-CD28 mAbs in *Hdac6*$^{-/-}$ was comparable to control, as determined by assessing PLCγ1 and erk1/2 (Erk1/2; also known as MAPK3 and MAPK1, respectively)phosphorylation (Fig. 1F). Likewise, the increase in intracellular calcium remained unchanged upon activation (Fig. 1G). As expected, tubulin acetylation at Lys40 was increased in *Hdac6*$^{-/-}$ CTLs (Fig. 1F). These results suggest that the killing defect observed does not result from a general impairment of CTLs function.

Defective *in vivo* and *ex vivo* killing in HDAC6 knockout mice

The effector activity of *Hdac6*$^{-/-}$ CD8^{+} T cells was tested *in vivo* following mouse immunization using SIINFEKL-pulsed dendritic cells. The *in vivo* killing activity against the injected target cells (pulsed or not with SIINFEKL) was analyzed upon recovery by peritoneal lavage. Notably, *Hdac6*$^{-/-}$ mice showed reduced specific killing of target cells (Fig. 2A, left panel). However, the proportion of SIINFEKL-specific CD8^{+} T cells from the endogenous repertoire was not affected in *Hdac6*$^{-/-}$ mice (Fig. 2A, right panel), suggesting that the cytotoxic function rather than the number of antigen-specific CTLs could underlie the defect. Next, we examined whether the decreased cytotoxic function of the CTLs resulted in an impaired ability to prevent morbidity and/or mortality during a viral infection. To restrict HDAC6 deficiency to CD8^{+} T cells, we adoptively transferred *Rag1*$^{-/-}$ mice with WT or *Hdac6*$^{-/-}$ naïve CD8^{+} T cells and subsequently challenged with a fully replicative vaccinia virus (VACV) WR strain. This infection model mimics the immunological and clinical features of smallpox vaccination in humans (Mota et al., 2011). CD8^{+} T cell proliferation was comparable, or even increased (division 4) in *Hdac6*$^{-/-}$ (Fig. 2B). *Rag1*$^{-/-}$ mice passively transferred with *Hdac6*$^{-/-}$ CD8^{+} T cells showed increased morbidity at 9 and 11 days post-infection (p.i.) (Fig. 2C). Virus titration from the lesion tissue demonstrated that *Hdac6*$^{-/-}$ immune cells exerted a less-efficient virus clearance (Fig. 2D). Consistent with our findings on the lack of effect in endogenous antigen-specific CD8^{+} T cell numbers, CTL expansion tracked at 13 d.p.i. was not affected in *Hdac6*$^{-/-}$ (Fig. 2E, left). The proportion of activated CD8^{+} T cells (CD44^{high}) at early (5 d.p.i) and late stages (13-30 d.p.i.) of the disease were similar for WT and *Hdac6*$^{-/-}$ mice (tested in peripheral blood and spleen, respectively; Fig. 2E, right). These *in vivo* results emphasize the role of HDAC6 in the CD8^{+} T cell-dependent protection against VACV infection without affecting effector CD8^{+} CTLs differentiation.

HDAC6 drives the terminal transport of LG to the target cell

CTL killing is limited to target cells (and not neighbor cells) by the confinement of secretion to the immune synapse established between the CTL and the target cell (de Saint Basile et al., 2010). Interestingly, the intracellular colocalization between cathepsinD and lamp1 (CD107a) was affected in *Hdac6*$^{-/-}$ CTLs conjugated with target cells, pointing to the mislocalization of lytic mediators in these cells (Fig. 3A; images and middle graphs). The decreased secretion of lytic proteins from *Hdac6*$^{-/-}$ CTLs suggests that HDAC6 regulates exocytosis of LG (Fig. 1C). Indeed, the translocation of the centrosome to the contact area with the target cell was even more pronounced in *Hdac6*$^{-/-}$ CTLs than in WT cells (Fig. 3A, right graph), in accordance with the effect described with the HDAC inhibitor Trichostatin A on the centrosomal polarization in CD4^{+} T cells (Serrador et al., 2004). This suggests that the defective exocytosis might rely on the movement of LG themselves.

We thus monitored the dynamics of LG at the subcortical immune synapse cytoskeleton and their release by Total Internal Reflection Fluorescence microscopy (TIRFm). CTLs were loaded with a pH-dependent, lysosomal tracker which allows the visualization of the LG and settled on to a stimulating surface to form an IS-like structure (Fig. 3B). These experiments revealed significant changes in the distribution of the LG and their dynamics, with a marked decrease in the number of LG detected at the immune synapse-like structure in *Hdac6*$^{-/-}$, suggesting alterations to the active transport of the granules from the centrosomal region to the plasma membrane. Indeed, the mean fluorescence intensity detected for *Hdac6*$^{-/-}$ granules was lower, which suggests a higher pH and therefore a different degree of maturation, although the LG displayed similar sizes in WT and *Hdac6*$^{-/-}$ cells (Fig. 3C). The most remarkable difference pertained to the *x*-*y* distribution of the LG, which was wider (diffusion surface) in the *Hdac6*$^{-/-}$ CTLs, with a higher diffusion coefficient, although maintaining similar duration times and path lengths (Fig. 3D). These data suggest that the LG from *Hdac6*$^{-/-}$ CTLs are not properly targeted and/or that they dock inefficiently at the immune synapse.

Tubulin motors control the delivery of LG to the plasma membrane. Whereas dynein controls LG targeting to the centrosome (Burkhardt et al., 1993; Mentlik et al., 2010), the kinesin-1/Slp3/Rab27a (Slp3 is also known as SYTL3) complex directs terminal transport to the plasma membrane for exocytosis (Kurowska et al., 2012). Dynactin might also be part of this complex, linking the cargo to kinesin-1 motor (Haghnia et al., 2007; Hendricks et al., 2010). We then hypothesized that HDAC6 regulates the movement and delivery of the LG at the IS through kinesin-1. Using a biochemical approach, we observed that HDAC6 formed a complex with kinesin-1 light chain (KLC1) upon triggering with anti-CD3 and anti-CD28 monoclonal antibodies (Fig. 3E). Moreover, interaction of the kinesin-activator complex dynactin subunits p150-glued (also known as DCTN1) and p50-dynamitin (also known as DCTN2) was impaired in *Hdac6*$^{-/-}$ (Fig. 3F).

In summary, our data support a specific role for HDAC6 in the intracellular localization of lytic mediators and, particularly, in their exocytosis. Therefore, the catalytic and scaffold activities of HDAC6 might act at multiple levels in the control of cytotoxic-related pathways, making HDAC6 a potential candidate that could be targeted to modulate CTLs in specific diseases.

Materials and Methods

Mice

Hdac6$^{-/-}$ mice were generated through targeting of exons 10 to 13 (Gao et al., 2007). They were intercrossed in a C57BL/6 background to generate wild-type and knockout littermates. Mice presenting transgenic inserts for mouse *Tcra*-Variable 2 and *Tcrb*-Variable 5 genes, which TCR recognizes ovalbumin$_{257-264}$ peptide in the context of H2Kb MHC-I (OT-I), were crossed to female *Hdac6*$^{+/-}$ mice to generate WT and KO littermates; males were used for *in vivo* experimentation since *Hdac6* is a X-linked gene. *Rag1*$^{-/-}$ mice were used for adoptive transfer experiments. These studies were approved by the local Ethics Committee for Basic Research at the CNIC and the Comunidad Autónoma de Madrid.

Cell culture

Cytotoxic cells were produced by culturing cells upon stimulation with SIINFEKL peptide (0.5 μM, 24h) or concanavalin A (2.5 μg/ml, 36 h) and cultured in presence of IL-2 (50-100 IU/ml) for at least 7 days. All other cells were cultured and treated as described previously (Cascio et al., 2015; Martin-Cofreces et al., 2006; Sancho et al., 2008).

Immunoprecipitation, CTL signaling and immunoblotting

Experimentation was performed as described (Martin-Cofreces et al., 2012; Martin-Cofreces et al., 2008; Martin-Cofreces et al., 2006).); KLC1 antibody was from Merck Millipore (5 μg/ml for Immunoprecipitation and 1 μg/ml for Western blot; Darmstadt, Germany; KLC), anti-HDAC6 from Assay Biotech (0.1 μg/ml for Western blot; Sunnyvale, California, US) and anti-p50 (0.25 μg/ml for Western blot) and -p150 (1 μg/ml for Immunoprecipitation and 0.25 μg/ml) for Western blot from BD Pharmingen (Franklin Lakes, New Jersey,US).

Measurement of intracellular variations in Calcium ions by flow cytometry

The method used for intracellular calcium influx is described (June and Moore, 2004). In particular, 5x10^6 purified CD8$^+$ CTLs generated *in vitro* were loaded with 2 μg.ml^{-1} INDO-1 AM (Invitrogen Corporation) and stimulated with anti-CD3 and anti-CD28 monoclonal antibodies (BD Biosciences; Franklin Lakes, New Jersey, US) plus goat anti-Armenian-hamster IgG antibodies (Jackson Immunoresearch Laboratories; West Grove, PA, US. 6, 3 and 6 μg/ml, respectively).

In vitro degranulation assay

CD107a expression was monitored with anti-CD107a-Alexa647 antibody (BD Biosciences) in monensin-pretreated CD8$^+$ OTI cells (5 mM) stimulated with SIINFEKL-pulsed EL4 (1 μM; 3 h, 37 ºC). Cells were stained with anti-CD8-PE and anti-CD44-FITC, analyzed by FACS and data were processed with FlowJo 7.6.5 (TreeStar Inc; Ashland, Oregon; US).

Confocal and Total Internal Reflection Fluorescence Microscopy analysis

Cell conjugates between CTLs and EL4 cells were allowed to form (15 min) and processed as described (Cascio et al., 2015; Martin-Cofreces et al., 2006) under a Leica SP5 confocal microscope (Leica Microsystems; Manheim, Germany) mounted on an inverted DMI6000

microscope fitted with a HCX PL APO 63x/1.40-0.6 oil objective. Images were processed using Imaris software (Bitplane; Zurich, Switzerland), Image J software (http://rsbweb.nih.gov/ij/) and assembled with Photoshop 6 software. 3D distance from the centrosomal centre of mass to the target cell-edge was measured by generating image masks from fluorescence with Imaris Software. TIRFm imaging was performed with a Leica AM-TIRF-MC-M system mounted on a Leica DMI-6000B microscope coupled to an Andor-DU8285_VP-4094 camera (Andor; Belfast, UK) fitted with a HCX-PL-APO 100.0x1.46 OIL objective as described (Baixauli et al., 2011; Martin-Cofreces et al., 2012). The laser penetrance used was 90 nm (561 nm laser). The LG mechanical properties were determined with a user-customized routine developed in Python. The software can be freely downloaded from: https://dl.dropboxusercontent.com/u/4050954/VesiclesAnalyser.zip. For more information, see the tutorial included.

Vaccinia virus (VACV) infection and virus titration

Tails were scarified with VACV ($2x10^6$ PFU/mouse) by gently scratching (x25) with a 28 1/2 G needle. For virus titration, tails were mechanical disaggregated (1ml of PBS), subjected to freeze-thaw cycles and sonication. Serial dilutions of the homogenates were added to monolayers of CV-1 cells seeded in 24 well plates. Cells were stained with Cristal violet 24 h later. We observed a detection limit of 5 PFU/tail, the number of plaques was multiplied by the reciprocal of sample dilution and converted to p.f.u./g of tissue.

In vitro and *in vivo* cytotoxicity assay

For *in vitro* experiments, EL4 target cells were incubated with 1 μM Cell Violet pulsed with 1 μM SIINFEKL or with 0.1 μM Cell Violet and no SIINFEKL, washed extensively, mixed (1:1), pooled with different dilutions of effectors, plated in a 96-well U-bottom plate for 5 h (37ºC) by triplicate and analyzed by FACS. Dead cells were excluded on the basis of propidium iodide staining. The mean percentage of survival in antigen-loaded targets was calculated relative to antigen-negative internal controls in each sample. Specific lysis was calculated using the following equation: percentage specific lysis = 100 * (1 - (percentage of cells staining for Cell Violet 1μM/percentage of cells staining for Cell Violet 0,1μM). All data were normalized to the basal specific lysis in absence of effector cells. For *in vivo* assays, WT and *Hdac6*$^{-/-}$ mice were immunized by i.p. injection of bone marrow dendritic cells pulsed with 1 μM of SIINFEKL and LPS (1 $\mu g ml^{-1}$) for 1 h. After 7 days, CD45.1 splenocytes were prepared as targets as described above and injected i.p. into recipients. Cells were recovered 24 h later by peritoneal lavage and *in vivo* killing measured (Hermans et al., 2004; Iborra et al., 2012; Sancho et al., 2008; Schulz et al., 2005).

Statistical analysis

Data were analyzed with GraphPad Prism software (La Jolla, California, US) for normality (D'Agostino-Pearson or the Kolmogorov-Smirnov test for small sAMples). Student's *t*-tests or Mann-Whitney tests were used for normal or non-normal data, respectively and two-tailed ANOVA for grouped data (Bonferroni post-test).

Europe PMC Funders Author Manuscripts

Supplementary Material

Refer to Web version on PubMed Central for supplementary material.

Acknowledgements

We thank Manuel Gomez and Miguel Vicente for critical reading of the manuscript. Experimentation was performed at Cellomics and Microscopy Units (CNIC) and Flow Cytometry Core Unit (CNIO).

Funding. This work was supported by the Ministerio de Economía y Competitividad (MINECO) [grant number SAF2014-55579-R], CAM [grant numbers INDISNET01592006, BIOMID-PIE13/041 and RD12/0042/0056]; from Universidad Carlos III de Madrid; and FEDER and ERC-2011-AdG 294340-GENTRIS. CNIC is supported by the MINECO and Pro-CNIC Foundation.

References

Baixauli F, Martin-Cofreces NB, Morlino G, Carrasco YR, Calabia-Linares C, Veiga E, Serrador JM, Sanchez-Madrid F. The mitochondrial fission factor dynamin-related protein 1 modulates T-cell receptor signalling at the immune synapse. The EMBO journal. 2011; 30:1238–50. [PubMed: 21326213]

Burkhardt JK, McIlvain JM Jr, Sheetz MP, Argon Y. Lytic granules from cytotoxic T cells exhibit kinesin-dependent motility on microtubules in vitro. Journal of cell science. 1993; 104(Pt 1):151–62. [PubMed: 8449993]

Cabrero JR, Serrador JM, Barreiro O, Mittelbrunn M, Naranjo-Suarez S, Martin-Cofreces N, Vicente-Manzanares M, Mazitschek R, Bradner JE, Avila J, et al. Lymphocyte chemotaxis is regulated by histone deacetylase 6, independently of its deacetylase activity. Molecular biology of the cell. 2006; 17:3435–45. [PubMed: 16738306]

Cascio G, Martin-Cofreces NB, Rodriguez-Frade JM, Lopez-Cotarelo P, Criado G, Pablos JL, Rodriguez-Fernandez JL, Sanchez-Madrid F, Mellado M. CXCL12 Regulates through JAK1 and JAK2 Formation of Productive Immunological Synapses. Journal of immunology. 2015; 194:5509–19.

de Saint Basile G, Menasche G, Fischer A. Molecular mechanisms of biogenesis and exocytosis of cytotoxic granules. Nature reviews Immunology. 2010; 10:568–79.

de Zoeten EF, Wang L, Butler K, Beier UH, Akimova T, Sai H, Bradner JE, Mazitschek R, Kozikowski AP, Matthias P, et al. Histone deacetylase 6 and heat shock protein 90 control the functions of Foxp3(+) T-regulatory cells. Molecular and cellular biology. 2011; 31:2066–78. [PubMed: 21444725]

Gao YS, Hubbert CC, Lu J, Lee YS, Lee JY, Yao TP. Histone deacetylase 6 regulates growth factor-induced actin remodeling and endocytosis. Molecular and cellular biology. 2007; 27:8637–47. [PubMed: 17938201]

Haghnia M, Cavalli V, Shah SB, Schimmelpfeng K, Brusch R, Yang G, Herrera C, Pilling A, Goldstein LS. Dynactin is required for coordinated bidirectional motility, but not for dynein membrane attachment. Molecular biology of the cell. 2007; 18:2081–9. [PubMed: 17360970]

Hendricks AG, Perlson E, Ross JL, Schroeder HW 3rd, Tokito M, Holzbaur EL. Motor coordination via a tug-of-war mechanism drives bidirectional vesicle transport. Current biology: CB. 2010; 20:697–702. [PubMed: 20399099]

Hermans IF, Silk JD, Yang J, Palmowski MJ, Gileadi U, McCarthy C, Salio M, Ronchese F, Cerundolo V. The VITAL assay: a versatile fluorometric technique for assessing CTL- and NKT-mediated cytotoxicity against multiple targets in vitro and in vivo. J Immunol Methods. 2004; 285:25–40. [PubMed: 14871532]

Hubbert C, Guardiola A, Shao R, Kawaguchi Y, Ito A, Nixon A, Yoshida M, Wang XF, Yao TP. HDAC6 is a microtubule-associated deacetylase. Nature. 2002; 417:455–8. [PubMed: 12024216]

Iborra S, Izquierdo HM, Martinez-Lopez M, Blanco-Menendez N, Reis e Sousa C, Sancho D. The DC receptor DNGR-1 mediates cross-priming of CTLs during vaccinia virus infection in mice. The Journal of clinical investigation. 2012; 122:1628–43. [PubMed: 22505455]

Europe PMC Funders Author Manuscripts

June CH, Moore JS. Measurement of intracellular ions by flow cytometry. Curr Protoc Immunol. 2004; Chapter 5 Unit 5 5.

Kawaguchi Y, Kovacs JJ, McLaurin A, Vance JM, Ito A, Yao TP. The deacetylase HDAC6 regulates aggresome formation and cell viability in response to misfolded protein stress. Cell. 2003; 115:727–38. [PubMed: 14675537]

Kurowska M, Goudin N, Nehme NT, Court M, Garin J, Fischer A, de Saint Basile G, Menasche G. Terminal transport of lytic granules to the immune synapse is mediated by the kinesin-1/Slp3/Rab27a complex. Blood. 2012; 119:3879–89. [PubMed: 22308290]

Lopez JA, Jenkins MR, Rudd-Schmidt JA, Brennan AJ, Danne JC, Mannering SI, Trapani JA, Voskoboinik I. Rapid and unidirectional perforin pore delivery at the cytotoxic immune synapse. Journal of immunology. 2013; 191:2328–34.

Martin-Cofreces NB, Baixauli F, Lopez MJ, Gil D, Monjas A, Alarcon B, Sanchez-Madrid F. End-binding protein 1 controls signal propagation from the T cell receptor. The EMBO journal. 2012; 31:4140–52. [PubMed: 22922463]

Martin-Cofreces NB, Robles-Valero J, Cabrero JR, Mittelbrunn M, Gordon-Alonso M, Sung CH, Alarcon B, Vazquez J, Sanchez-Madrid F. MTOC translocation modulates IS formation and controls sustained T cell signaling. The Journal of cell biology. 2008; 182:951–62. [PubMed: 18779373]

Martin-Cofreces NB, Sancho D, Fernandez E, Vicente-Manzanares M, Gordon-Alonso M, Montoya MC, Michel F, Acuto O, Alarcon B, Sanchez-Madrid F. Role of Fyn in the rearrangement of tubulin cytoskeleton induced through TCR. Journal of immunology. 2006; 176:4201–7.

Mentlik AN, Sanborn KB, Holzbaur EL, Orange JS. Rapid lytic granule convergence to the MTOC in natural killer cells is dependent on dynein but not cytolytic commitment. Molecular biology of the cell. 2010; 21:2241–56. [PubMed: 20444980]

Mosley AJ, Meekings KN, McCarthy C, Shepherd D, Cerundolo V, Mazitschek R, Tanaka Y, Taylor GP, Bangham CR. Histone deacetylase inhibitors increase virus gene expression but decrease CD8+ cell antiviral function in HTLV-1 infection. Blood. 2006; 108:3801–7. [PubMed: 16912225]

Mota BE, Gallardo-Romero N, Trindade G, Keckler MS, Karem K, Carroll D, Campos MA, Vieira LQ, da Fonseca FG, Ferreira PC, et al. Adverse events post smallpox-vaccination: insights from tail scarification infection in mice with Vaccinia virus. PloS one. 2011; 6:e18924. [PubMed: 21526210]

Pardo J, Aguilo JI, Anel A, Martin P, Joeckel L, Borner C, Wallich R, Mullbacher A, Froelich CJ, Simon MM. The biology of cytotoxic cell granule exocytosis pathway: granzymes have evolved to induce cell death and inflammation. Microbes and infection / Institut Pasteur. 2009; 11:452–9. [PubMed: 19249384]

Ritter AT, Angus KL, Griffiths GM. The role of the cytoskeleton at the immunological synapse. Immunological reviews. 2013; 256:107–17. [PubMed: 24117816]

Sancho D, Mourao-Sa D, Joffre OP, Schulz O, Rogers NC, Pennington DJ, Carlyle JR, Reis e Sousa C. Tumor therapy in mice via antigen targeting to a novel, DC-restricted C-type lectin. J Clin Invest. 2008; 118:2098–110. [PubMed: 18497879]

Schulz O, Diebold SS, Chen M, Naslund TI, Nolte MA, Alexopoulou L, Azuma YT, Flavell RA, Liljestrom P, Reis e Sousa C. Toll-like receptor 3 promotes cross-priming to virus-infected cells. Nature. 2005; 433:887–92. [PubMed: 15711573]

Serrador JM, Cabrero JR, Sancho D, Mittelbrunn M, Urzainqui A, Sanchez-Madrid F. HDAC6 deacetylase activity links the tubulin cytoskeleton with immune synapse organization. Immunity. 2004; 20:417–28. [PubMed: 15084271]

Tsuji G, Okiyama N, Villarroel VA, Katz SI. Histone deacetylase 6 inhibition impairs effector CD8 T-cell functions during skin inflammation. The Journal of allergy and clinical immunology. 2015; 135:1228–39. [PubMed: 25458911]

Valenzuela-Fernandez A, Cabrero JR, Serrador JM, Sanchez-Madrid F. HDAC6: a key regulator of cytoskeleton, cell migration and cell-cell interactions. Trends in cell biology. 2008; 18:291–7. [PubMed: 18472263]

Williams MA, Bevan MJ. Effector and memory CTL differentiation. Annual review of immunology. 2007; 25:171–92.

Zhang X, Yuan Z, Zhang Y, Yong S, Salas-Burgos A, Koomen J, Olashaw N, Parsons JT, Yang XJ, Dent SR, et al. HDAC6 modulates cell motility by altering the acetylation level of cortactin. Molecular cell. 2007; 27:197–213. [PubMed: 17643370]

Europe PMC Funders Author Manuscripts

Europe PMC Funders Author Manuscripts

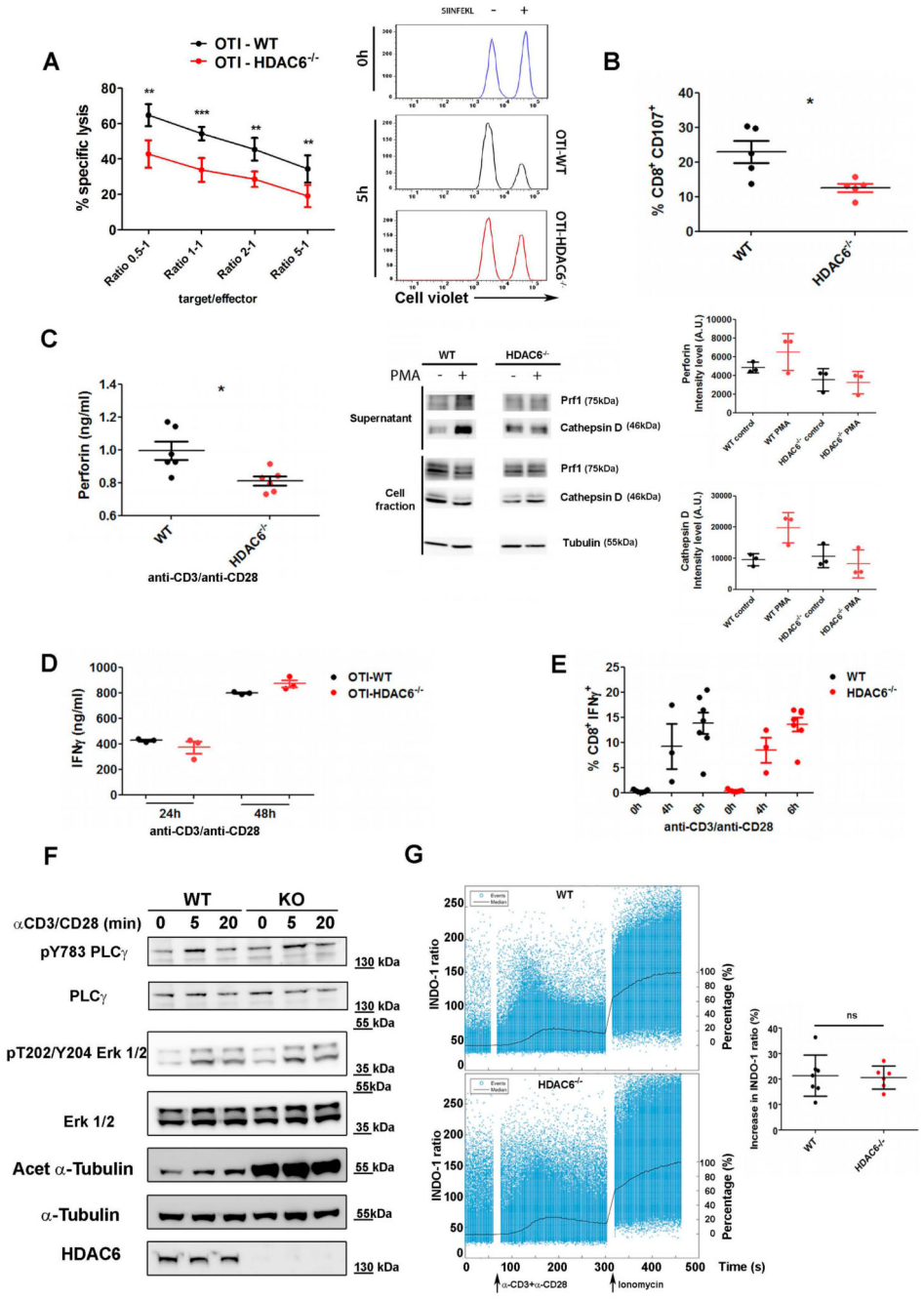

Figure 1. HDAC6 modulates the efficiency of target cell killing and degranulation of lytic mediators.

(A) Graph showing *in vitro* cytotoxic assay for specific lysis of SIINFEKL-pulsed EL4 target cells by OT-I-WT or -*Hdac6*$^{-/-}$ CTLs. Mean ± SEM of specific lysis for 5 h are shown at the indicated target to effector ratios. All killing assay where performed by triplicate. *, P < 0.05; **, P < 0.01; ***, P < 0.001. Unpaired T-test (n=5 mice for each genotype). Histograms, representative FACS profile. (B) Degranulation is shown as the percentage of CD107a^{+} cells detected by FACS in activated vs non-stimulated WT and *Hdac6*$^{-/-}$ CD8^{+} CTLs. Results are mean±s.e.m. n=5 for each genotype. (C) Exocytosis of lytic mediators

upon T cell activation. Left, Perforin content in culture cell supernatants was determined by ELISA. CTLs were stimulated with anti-CD3 and anti-CD28 monoclonal antibodies and 'goat' anti-Armenian-hamster 'IgG' anyibodies (5 h). Graphs show mean±s.e.m. (n=6 mice for each genotype). *P<0.05 (unpaired t-test). Middle panel, representative Western blot showing exocytosis. PMA stimulation (1 h). Normalization was performed against cell fractions. Right graphs, Mean +/-SEM (3 independent experiments). (D) Graph, IFNγ secretion supernatants from anti-CD3/anti-CD28 mAbs activated WT and *Hdac6*$^{-/-}$ CTLs by ELISA. Results are mean±s.e.m. n=3 for each genotype. Mann-Whitney test. (E) Percentage of IFNγ^{+} cells in WT and *Hdac6*$^{-/-}$ CTLs activated with anti-CD3 and anti-CD28 monoclonal antibodies. Results are mean±s.e.m. n=6 (0 and 6 h) and n= 3 (4 h) for each genotype. Mann-Whitney test. (F) Effector CD8^{+} CTLs isolated from WT and *Hdac6*$^{-/-}$ mice were activated (anti-CD3/anti-CD28 mAbs), lysed and blotted against PLCγ1 (pY783) and erk1/2 (pT202/Y204) phosphorylation and tubulin acetylation. (G) Calcium flux. WT and *Hdac6*$^{-/-}$ purified CTLs pre-loaded with the INDO-1 AM probe were analyzed for free and bound Ca^{2+} by flow cytometry. Left graphs, time course ratiometric variation (left Y axis). Black line, Median function normalized to basal (0%) and total activation by ionomycin treatment (100%; right Y axis). Stimuli are indicated. A representative experiment is shown. Right graph, Mean of the increase in the ratio +/-SD (WT, n=7; *Hdac6*$^{-/-}$ n=6. Mann Whitney test).

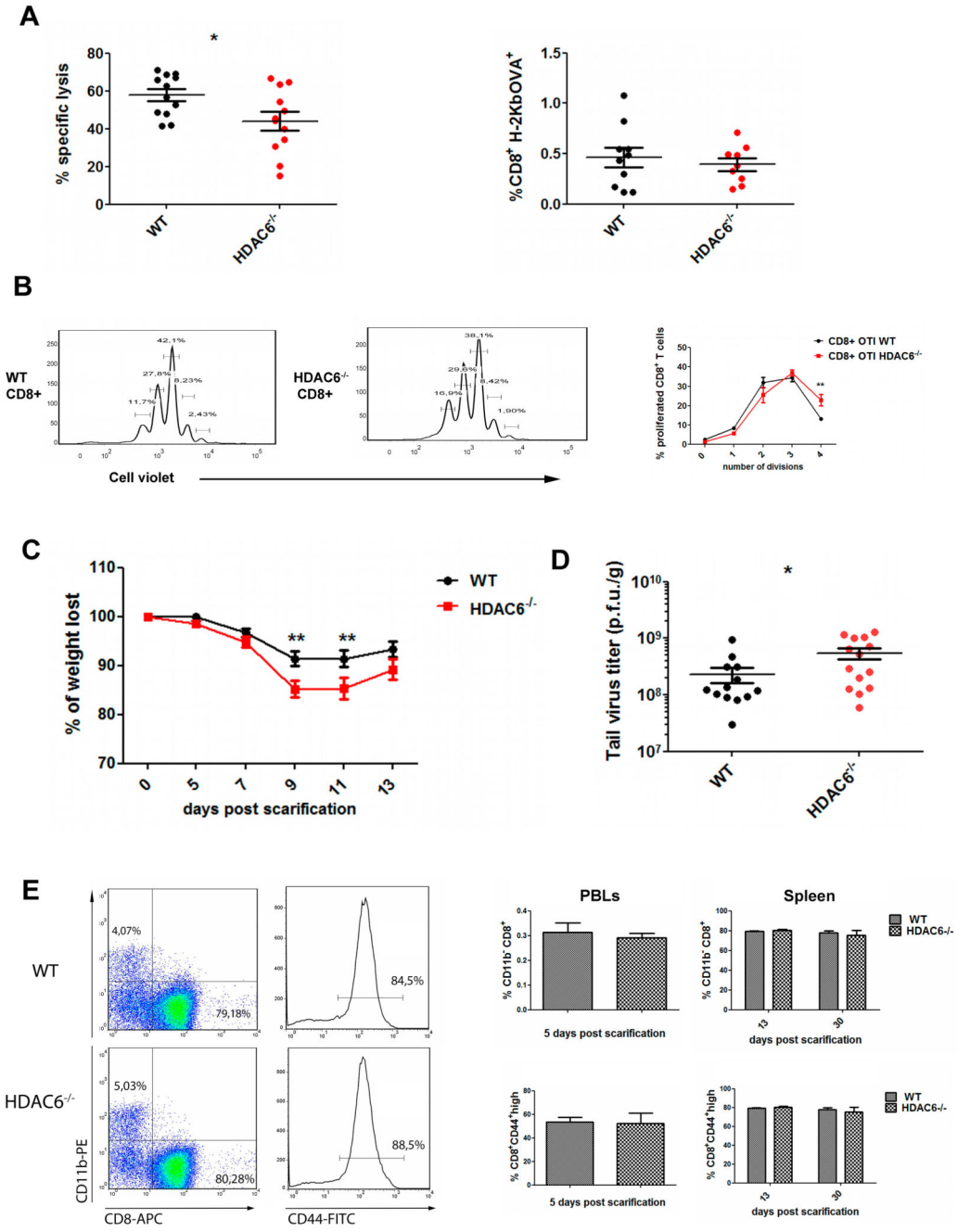

Figure 2. In vivo function of CTLs is impaired in HDAC6 knockout mice.

(A) WT and *Hdac6*$^{-/-}$ were immunized against SIINFEKL peptide. 7 days after immunization, cell violet-labelled, SIINFEKL-pulsed or not target cells (1 μM) were injected i.p., recovered through intraperitoneal lavage (24 h) and cell survival assessed by FACs (left panel). Data represent mean±s.e.m. (n= 12 for each genotype from three independent experiments). *P<0.05, Mann-Whitney test. Relative percentage of $CD8^+$ $H\text{-}2Kb^+$ was determined to control avidity towards SIINFEKL (right panel, results are mean ±s.e.m. (WT, n= 10; *Hdac6*$^{-/-}$, n= 9 from three independent experiments. Mann-Whitney's

Europe PMC Funders Author Manuscripts

test). (B) Proliferation of $CD8^+$ cells in VACV-OVA infected WT and *Hdac6*$^{-/-}$ mice. Results are means±s.e.m. (n= 5 for each genotype). **P<0.01 (Mann-Whitney test). (C) *Rag1*$^{-/-}$ mice inoculated i.v. with $0.8x10^6$ $CD8^+$ naïve cells and infected with VACV-WR by tail scarification were weighted every 2 days. Results are means±s.e.m. (n=10 for each genotype). **P<0.01 (Mann-Whitney test). (D) Titration of viral particles from scarified tails (13 d.p.i). The colonies of CV-1 cells infected *in vitro* with different dilutions of tail extracts were counted, and normalized to the tail tissue weight. Results are means±s.e.m. (WT, n= 13; *Hdac6*$^{-/-}$ n= 14). *P<0.05 (Mann-Whitney test). (E) Percentage of $CD8^+$ expansion and CD44 expression by FACs analysis in peripheral blood (5 d.p.i) and in spleen populations (13 and 30 d.p.i.). CD11b was used as negative control. Results are means ±s.e.m. (n= 5) (Mann-Whitney test).

Europe PMC Funders Author Manuscripts

Europe PMC Funders Author Manuscripts

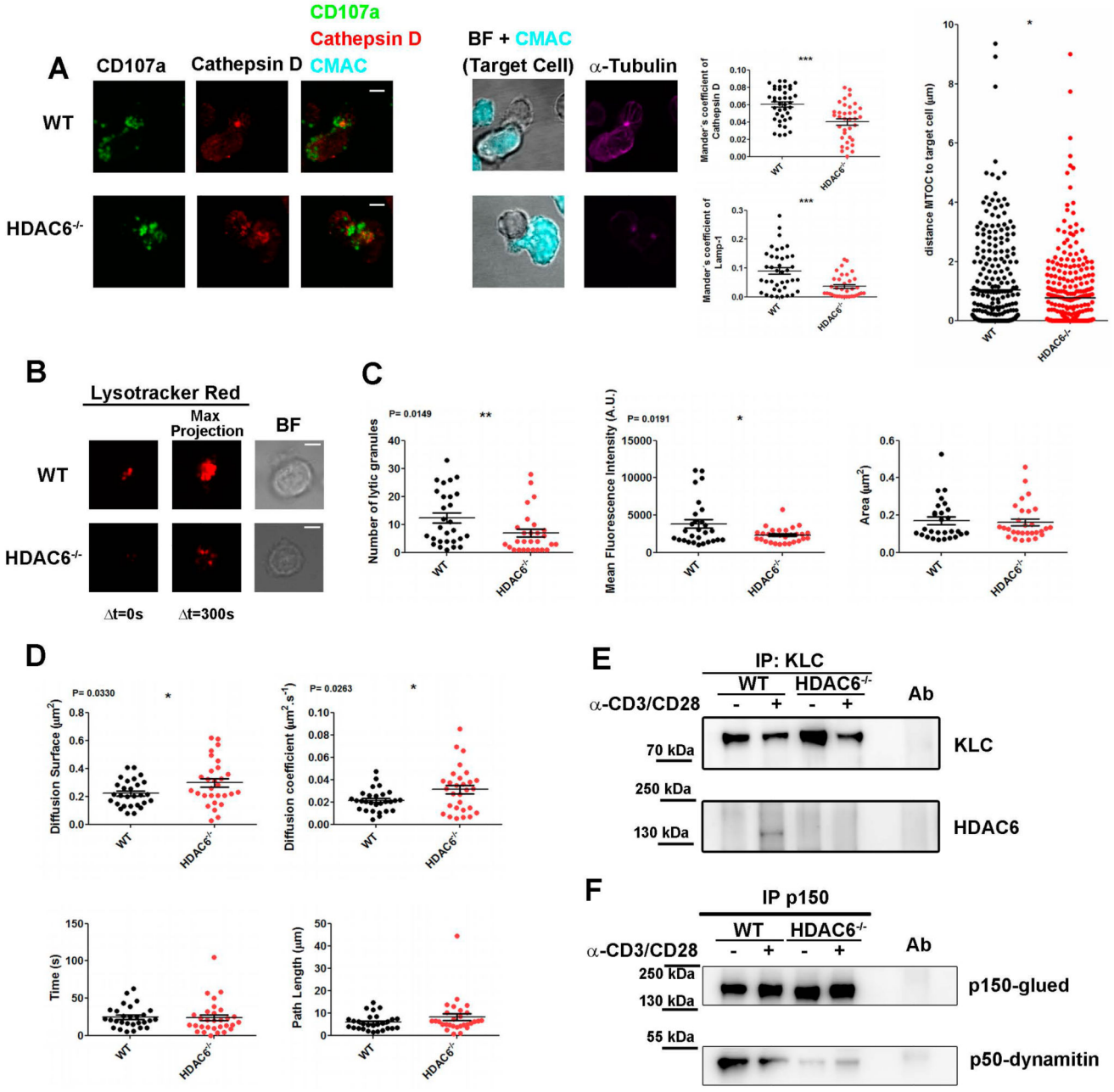

Figure 3. HDAC6 drives the terminal transport of LG to the target cell.

(A) Confocal microscopy images of WT and *Hdac6*$^{-/-}$ OT-I-derived CTLs conjugated with CMAC-loaded, OVA pre-pulsed target cell EL4 (500 nM SIINFEKL, Cyan) for 15 min. Green, CD107a. Red, CathepsinD. Magenta, α-tubulin. Bright-field (BF) images correspond to a unique plane and fluorescence images, to maximal projections from Z-stacks. Middle graphs, Mander's coefficient for co-localization of Lamp1 and CathepsinD. Results are mean±???? (WT, n=39; Hdac6−/−, n=35). ***P<0.001 (Mann–Whitney test). Right graph, quantification of MTOC translocation. Results are mean±s.e.m. (n>270, from 3 independent experiments); *P<0.05 (unpaired *t*-test). (B) Representative TIRFm images of Lysotracker

Red-loaded WT and *Hdac6*$^{-/-}$ CTLs in glass-bottom chambers coated with anti-CD3 and anti-CD28 monoclonal antibodies. Video recording was initiated upon cell adhesion (37ºC and 5% CO_2). Images were acquired for 5 min every 0.5 s. (C-D) Quantification for LG parameters at the IS-like was performed for each cell Results are means±s.e.m. (n=28 for each genotype, 3 independent experiments). *P<0.05; **P<0.01. Mann-Whitney test. (E-F) Western blots showing immunoprecipitates from resting or activated WT and *Hdac6*$^{-/-}$ CTLs (15 min) from a representative experiment out of three. Antibodies anti-KLC1 (E) or anti-p150 glued (p150) were used (F). Samples were blotted against indicated antibodies. Ab, pre-immune control antibody. Scale bars: 4 μm.